STRATEGIES FOR MARS NETWORK SCIENCE MISSIONS VIA INNOVATIVE AEROCAPTURE AND EDL ARCHITECTURES

Sarag. J. Saikia[(1)], Blake Rogers[(1)], James M. Longuski[(1)], Harish Saranathan[(1)], and Michael J. Grant[(1)]

[(1)]School of Aeronautics & Astronautics, Purdue University, 701 West Stadium Ave., IN 47907-2045, U.S.A.
Email:sarag@purdue.edu

ABSTRACT

A method of delivering four landers to Mars with a separation of 3000 km using a single Atlas-Centaur is presented. The architecture consists of two identical flight systems, each composed of two Phoenix-class spacecraft, a cruise stage, and an extended drag skirt. The Centaur (or an ion propulsion system) provides the necessary ΔV to achieve the required minimum seven-day separation between entries of the two flight systems. In the entry of each flight system, the drag skirt is attached to one of the spacecraft to create the differential drag needed to achieve the landing separation. Monte Carlo simulations demonstrate acceptable performance of the architecture for dispersions in atmospheric density, flight path angle, velocity, mass, drag coefficients, and spacecraft jettison time.

1. INTRODUCTION

According to the Decadal Survey [1] and Mars Exploration Program Analysis Group (MEPAG) [2], one of the strongest needs of Mars exploration is to characterize the near-surface weather and climate, understand the large-scale atmospheric dynamics, and explore the interior structure and composition—referred to as Mars network science objectives. The composition, structure, and history of Mars are crucial in the studies of the Solar System and will lead to understanding the processes that have influenced the evolution of the rocky planets of the inner solar system including that of Earth. Previous missions have probed the surface of Mars, mostly concentrating on features such as volcanoes, canyons, rocks, and soil. However, no attempt has been made to study the planet's earliest evolution by making sub-surface and seismic measurements. Concurrent geophysical measurements at multiple locations on Mars surface are highly desirable for science investigations, and it is most crucial to have such a grid of stations for a network.

In the past, several missions have been proposed—NetLander [3], Mars Network Science Mission [4], MetNet [5] for Mars network science missions, but have been restricted to design phase only. JPL's Team X conducted a full mission study in response to the Decadal Survey where a two-lander mission concept was selected [6]. InSight mission [7] is expected to be launched in March 2016 under NASA's Discovery Program which would place a single geophysical lander on Mars to study its deep interior. The mission relies on Phoenix Mars lander and other proven technologies to reduce risk and cost. The mission also capitalizes on advances in technology and analysis to obtain the same results using one lander that previously required four stations. However, a network of four stations will enable greater science return than possible via the InSight mission.

2. MISSION CONCEPT AND ARCHITECTURE

The architecture consists of two identical and independent flight systems. Each flight system comprises of four flight elements—primary and secondary spacecraft, two entry systems, single cruise stage, and an adapter and release mechanism between the primary and secondary spacecraft. Both the spacecraft in a flight system are identical Phoenix-class aeroshell, but the primary spacecraft has a heat shield extension (drag skirt). The size of the drag skirt is constrained by the diameter of the payload fairing of the Atlas V 541. For this study, 5 m diameter Extra Extended Payload Fairing (XEPF) or Extended Payload Fairing (EPF) are considered [8]; although Atlas V Heavy Lift Vehicle, in future, may have payload fairing with diameter up to 7.2 m [8]. Constraint posed by the fairing diameter primarily affects the size of extended heat shield.

The goal of this study is to deliver four Mars Phoenix-class landers with a separation of 3,000 km between them, with a single launch from Earth—as shown in Fig. 1. The concept uses an alternative EDL architecture to land two spacecraft with a single Mars entry and a total of four spacecraft with two Mars entries, all using a single rocket launch from Earth.

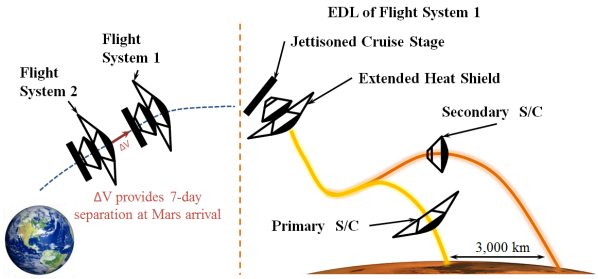

Fig. 1: Mission architecture concept in which four landers are delivered on to Mars surface with a single-launch from Earth.

2.1 Launch Configuration

Since there are two identical flight systems and each flight system in turn includes two spacecraft, a two-lander stacked-configuration is considered as in Fig. 2. The two flight systems are then stacked using a Dual Payload Carrier [8]. In each flight system, the two spacecraft are stacked using a common carrier element.

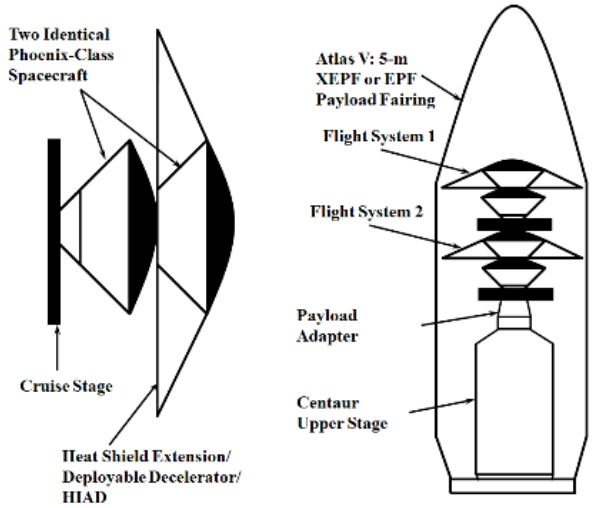

Fig. 2: On left hand side is the cruise configuration of one Flight System, and on the right hand side is the launch configuration of the two flight systems.

The Centaur upper stage (3 m diameter, 10 m length), payload adapters, and two flight systems are stacked inside the Atlas V 5m diameter XEPF (26.5 m length) or EPF (23. 5 m length). The selection of stacked configuration leads to increase of flight systems and well as spacecraft separation failure, but such risks could be mitigated.

2.2 Cruise Stage Configuration

A common carrier which is capable of delivering the two landers to Mars is considered for each flight system. The carrier also contains a mechanism to jettison the secondary spacecraft from the flight system at an appropriate point of the entry trajectory to achieve the range separation requirement. Only a single cruise stage is used for both the spacecraft in each flight system; however, this necessitates a complex carrier element.

2.2 Drag Skirt Options

The primary spacecraft's ballistic coefficient is lower than the secondary spacecraft to achieve a range separation of around 3000 km. The ballistic coefficient is lowered via increased drag area using an extended drag skirt. Three options for drag skirt are considered keeping in mind the present capabilities and future possibilities. These are (a) Heat Shield Extension (b) Rigid Deployable Decelerator (RDD) (c) Hypersonic Inflatable Aerodynamic Decelerator (HIAD). For all the options, it is assumed that the 70-deg cone geometry is preserved for simplicity. The length of the drag skirt is extended increasing the outer diameter to fit in to the payload fairing of 5 m. Heat shield extension does not require in-space deployment prior to entry and is feasible with current technologies. Thus the drag area of the extended drag skirt option could be equal to or lower as compared to RDD and HIAD options.

2.3 Instrument Payloads

Science payload mass of around 60 kg is assumed in consistent with the Phoenix mission [9]. JPL's Team X's study on Mars Geophysical Network Mission [7], on the other hand, considered a total of 25 kg including 30% reserves. While the details are not worked out, a 60 kg science payload can accommodate a wide array of science instruments—seismometer, instrument deployment arm, instrument deployment camera, surface stereo camera, atmospheric instrument suite, X-band transponder, heat flow probe, dust opacity and concentration instruments, an electromagnetic sounder, a humidistat, and sonic anemometers. A detailed description of these instruments can be found in [7]. Inclusion of this array of instruments will enable enhanced science to address the goals of a Mars network science mission.

2.4 Mission Mass

The maximum expected mass (MEM) of each flight system is estimated to be around 1380 kg (including a 2% reserve). The MEM includes two Phoenix-class spacecraft, two backshells, one parachute, an extended

drag skirt for the primary spacecraft, a cruise stage, a heat shield on the secondary spacecraft, propellant, solar electric propulsion (optional), and secondary spacecraft adapter and release mechanism. Therefore, the total MEM is 2800 kg (similar to the entry mass of the Mars Science Laboratory mission), which is within the capability of the Atlas V 541 launch vehicle.

3. SINGLE-EVENT DRAG MODULATION

A single-event drag modulation is performed by releasing the secondary spacecraft from a flight system at an appropriate instance. The release event instantaneously changes the ballistic coefficient of the primary (reduction in mass leads to decrease in β) and the secondary spacecraft (increase in drag area leads to increase in β). The appropriate time of secondary spacecraft release is selected to attain desired range separation as dictated by the mission requirements. The ballistic coefficient is larger than that of the primary spacecraft and less than that of the secondary spacecraft. Fig. 3 shows various vehicle configurations and the drag-modulation event.

3.1 Computation of Ballistic Coefficients and Drag Skirt Sizing

The mass and drag area of different decelerator devices are difficult to estimate. This section presents a more general approach of computing the ballistic coefficients of different vehicle configurations for a range of masses and drag areas of the extended drag skirt and examines the feasibility of this architecture.

The variables β_{fs}, β_p, and β_s are the ballistic coefficients of the flight system (without cruise stage), primary spacecraft, and secondary spacecraft respectively as shown in Fig. 3. Assume that m_{ds}, m_s are the masses, and $(C_D A)_{ds}$, $(C_D A)_s$, are the drag areas (product of drag coefficient and reference area) of the drag skirt (only), and the secondary spacecraft respectively.

$$\eta = \frac{m_{ds}}{m_s} \tag{1}$$

$$\kappa = \frac{(C_D A)_{ds}}{(C_D A)_s} \tag{2}$$

In Eqs. (1) and (2), η and κ serve as two simple design variables which are ratios of masses and drag areas of hypersonic drag skirt and secondary spacecraft respectively. The three ballistic coefficients are related to each other via the two variables, η and κ given by Eqs. 3-5.

$$\beta_{fs} = \frac{2+\eta}{1+\kappa}\,\beta_s \tag{3}$$

$$\beta_p = \frac{1+\eta}{1+\kappa}\,\beta_s \tag{4}$$

$$\beta_{ds} = \frac{2+\eta}{1+\eta}\,\beta_p \tag{5}$$

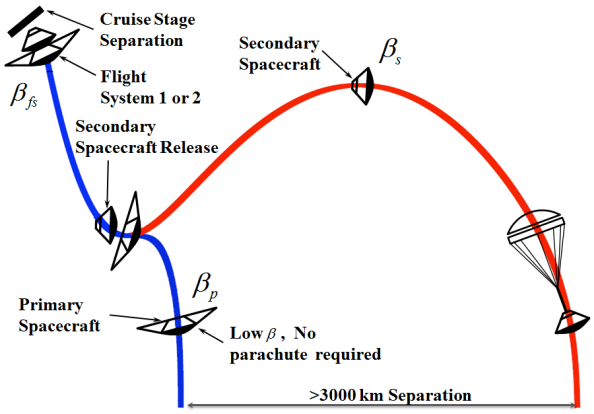

Fig. 3: Entry, descent, and landing timeline showing drag modulation event and various spacecraft configurations.

The values of ratios η and κ characterize the type of drag skirt. For the concept, it is found that $\beta_s > \beta_{fs} > \beta_p$, which is possible only when $\kappa > 1+\eta$. This constraint can be easily satisfied via one of the drag skirt options. Usually values of these two variables will be such that, $0 < \eta \le 1$ and $\kappa_{\min} < \kappa \le \kappa_{\max}$, where $\kappa_{\max}$ is a large positive integer such as 50. It is useful to note that $\eta = 0$ and $\kappa = 0$ signify the absence of any drag device. Designing a drag skirt for which $\eta = 1$, may not be realistic as it means that the mass of the drag skirt is same as the mass of the secondary spacecraft.

One way of designing will be to fix the value of β_s (selecting a particular spacecraft—Phoenix in this paper), and compute the values of β_{fs} and β_p for particular values of η and κ. The ratios of the ballistic coefficients in terms of β_s for the ranges of η and κ gives nonintersecting surfaces as shown in Fig. 4. The ballistic coefficient ratios depend strongly on the drag area ratio κ and weakly on the mass ratio, η. Therefore, considering a realistic value of the mass

ratio, $\eta = 0.2$, the two ballistic coefficient ratios (using Eqs. 3-4) are plotted as a function of κ only, as shown in Fig. 5.

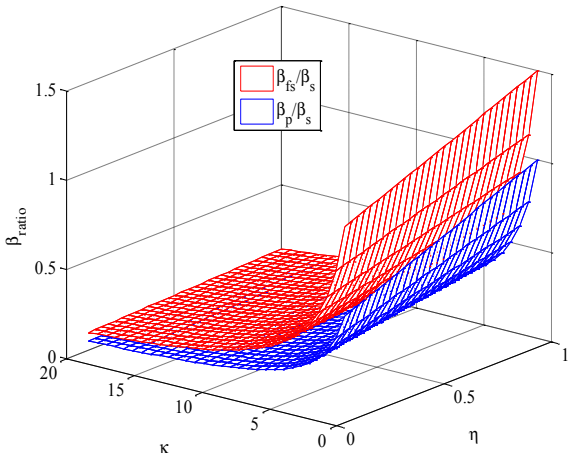

Fig. 4: Ballistic coefficient ratios as a function of design variables η and κ. The ballistic coefficient ratios show strong dependency on the variable κ and a weak dependency on η.

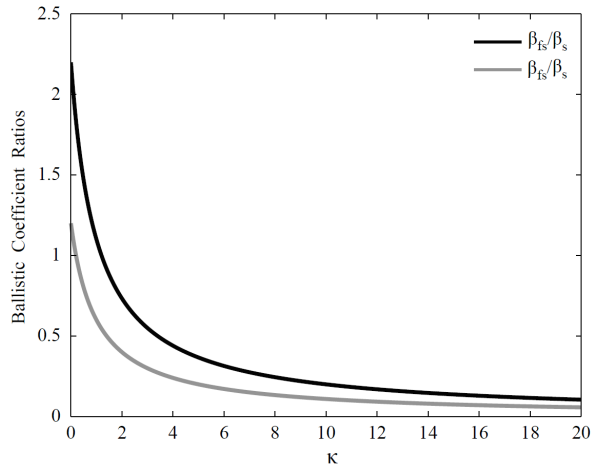

Fig. 5: Ballistic coefficient ratios as a function of drag area ratio κ for $\eta = 0.2$. The effects of ballistic coefficient ratios shrinks for $\kappa > 8$.

It is seen from Fig. 5 that the β ratios asymptotically decrease as κ is increased. Therefore, there are limits to which the ballistic coefficient ratios can be reduced by incorporating a drag skirt within the constraints posed by the launch vehicle payload fairing. Figure 5 shows that increasing κ_{max} (size of the drag skirt) does not offer significant advantages beyond a certain point. In other words, advantages of increasing the size of the drag skirt to reduce the ballistic coefficient ratios diminish for $\kappa > 8$.

4. INTERPLANETARY TRAJECTORY DESIGN

The Earth-to-Mars trajectories launch and arrival V_∞ are subject to constraints based upon the limitations of the launch vehicle and the EDL system, respectively. The maximum launch V_∞ for a mass of 1382 kg (of a flight system) using an Atlas V 541 with a Centaur upper stage is approximately 7 km/s [1].

To determine the maximum arrival V_∞, recall that the maximum entry speed for the EDL is desired to be approximately 6 km/s to suppress radiative heating. Entry occurs at an altitude of 125 km above the surface of Mars. If this altitude is the periapse of the hyperbola and the velocity is 6 km/s at this point, the V_∞ should be about 3.5 km/s. Therefore, the arrival V_∞ needs to be less than 3.5 km/s to minimize heating rate and heat load [10].

4.1 Ballistic Trajectories

The Satellite Tour Design Program (STOUR) developed by the Jet Propulsion Laboratory for the Galileo mission tour design [11] is used to get an initial guess for the Earth-to-Mars trajectory. STOUR uses an analytical ephemeris for the location of the planets and uses patched conics for interplanetary trajectories. Trajectories were found between January 1, 2020 and January 1, 2035. There were many results, but a representative cross section of the best results is shown in Table 1. The trajectories are below the 7 km/s limit for launch V_∞, but the one that launches on May 2, 2033 has a larger arrival V_∞ than desired.

Table 1: Ballistic Earth-Mars trajectories.

Launch Date	Launch V_∞	Arrival V_∞	Periapsis	Apoapsis	TOF
mm/dd/yy	km/s	Km/s	AU	AU	days
07/29/20	3.80	2.55	1.014	1.623	208
10/12/22	6.00	2.37	0.956	1.665	253
04/12/33	3.00	3.36	0.995	1.392	199
05/02/33	2.80	4.38	1.007	1.481	276

4.2 7-day Separation Trajectories

Two methods are considered to get the 7 day separation between the two spacecraft. The first method is to use the Centaur upper stage to give the second flight system an extra ΔV to separate the two flight system, and, thus, a slightly different interplanetary trajectory. The second method is to have low-thrust on the second flight system and shape the trajectory to arrive at least a week before or after the

ballistic trajectory. The low-thrust method has the added benefit of being capable of lowering the arrival V_∞ of the second flight system at Mars, thus making the EDL less costly.

Both of these types of trajectories are constructed using the Jet Propulsion Laboratory's Mission Analysis Low Thrust Optimization (MALTO) tool [12]. MALTO approximates continuous thrust by dividing each planet-planet leg of the trajectory into segments with an impulsive ΔV at each of the midpoints. The propagation of the trajectory between these impulsive maneuvers assumes conic trajectories and also assumes that all flybys are instantaneous and modeled by the rotation of the V_∞ vectors. This method results in a constrained nonlinear optimization problem, which MALTO solves by using the nonlinear programming software Sparse Nonlinear OPTimizer (SNOPT) [13]. The flight system is assumed to have the same propulsion system as Dawn spacecraft. The specific impulse is 3,100 s and a thrust level of 90 mN [14].

To find the trajectory required when the upper stage is used for separation, first the reference ballistic trajectory found in STOUR is re-created in MALTO. The launch date is then frozen and the arrival date is constrained to be 7 days before the arrival of the reference ballistic trajectory (the higher V_∞ at launch means a shorter time of flight) and another ballistic trajectory is found. The V_∞'s are not only different, but they are in slightly different directions, so we assume that the rocket is capable of putting each of the spacecraft on the correct orbit. Both of the trajectories in this case are ballistic, but their V_∞'s are slightly different from one another. The ΔV required does accrue some propellant cost during the upper stage, which is calculated using the rocket equation assuming an I_{sp} of 450 s.

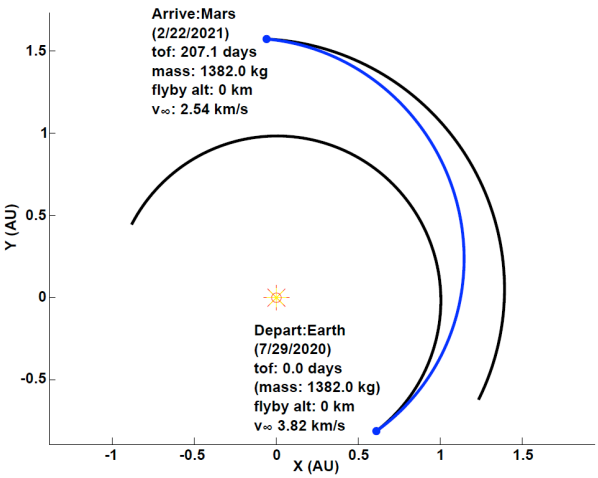

Fig. 6: Ballistic trajectory option.

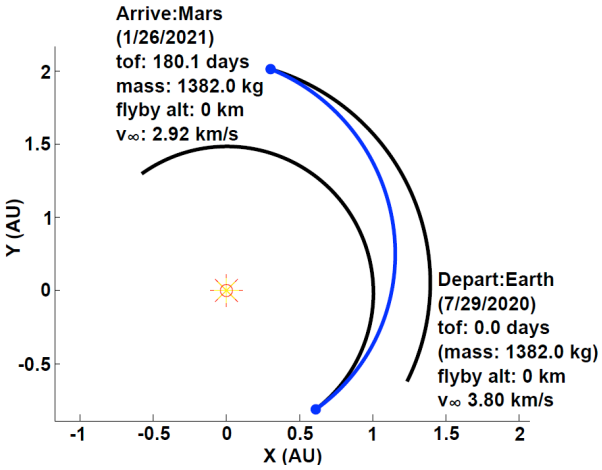

Fig. 7: Ballistic trajectory option with a ΔV using Centaur upper stage.

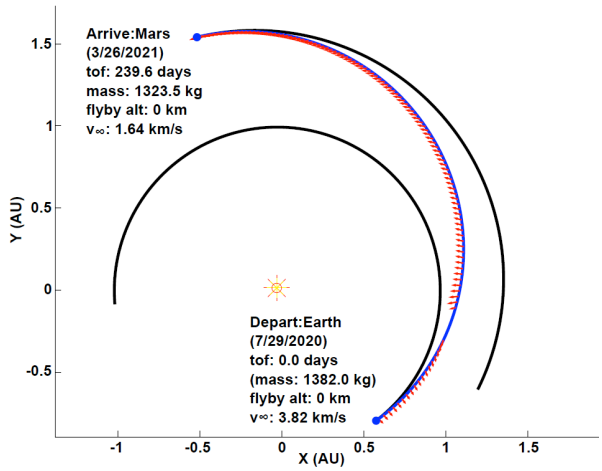

Fig. 8: Low-thrust trajectory option.

Table 2: Earth-Mars trajectory options using Centaur upper stage for separation maneuver.

Flight System	Launch Date	Arrival Date	Launch V∞	Arrival V∞	Centaur Propellant Required
Unit	mm/dd/yy	mm/dd/yy	(km/s)	(km/s)	kg
1	07/29/20	02/22/21	3.82	2.54	9.4
2	07/29/20	02/14/21	3.79	2.58	0
1	10/12/22	06/22/23	6.00	2.37	0
2	10/12/22	08/20/23	6.03	2.36	9.4
1	04/12/33	10/27/33	2.99	3.37	9.4
2	04/12/33	10/19/33	2.96	2.44	0

The properties of the trajectories can be seen in Table 2. As an example, the reference ballistic trajectory for July 29, 2020 and the corresponding ballistic trajectory with slightly altered launch V_∞ are shown in Figs. 6 and 7, respectively.

Finding the low-thrust trajectory entails taking the reference ballistic trajectory and then systematically lowering the constraints on arrival V_∞ until no propellant is left. The launch date and V_∞ Cartesian components are frozen while arrival date is required to be at least seven days before or after the arrival of the ballistic trajectory. The results of this effort are presented in Table 3. The low thrust trajectory found for a launch date of July 29, 2020 is shown in Fig. 4.

Table 3: Earth-Mars trajectory options using low thrust for separation maneuver.

Flight System	Launch Date	Arrival Date	Launch V∞	Arrival V∞	SEP Propellant Required
Unit	mm/dd/yy		(km/s)	(km/s)	kg
1	07/29/20	2/22/21	3.82	2.54	0
2	07/29/20	3/1/21	3.82	1.64	58.5
1	10/12/22	6/22/23	6.00	2.37	0
2	10/12/22	8/20/23	6.00	1.39	63.1
1	04/12/33	10/27/33	2.99	3.37	0
2	04/12/33	11/26/33	2.99	2.58	56.0

5. ENTRY, DESCENT, AND LANDING SIMULATION

A planar entry trajectory simulation program was coded in MATLAB and autocoded to C and compiled to enhance execution speed. An exponential atmosphere is used to evaluate the feasibility of the concept and to elucidate the capabilities. Mars-Gram 2005 is used as model for Mars' atmosphere based on altitude at equator for Monte Carlo uncertainty analysis. The effects of rotation of Mars, wind, and dust storms are not included in this study. Inverse-square gravity model is being used without any perturbative effects. For this architecture, ballistic flight of a spacecraft of mass m inside Mars' atmosphere is considered. The planet Mars is assumed to be non-rotating (and no winds) with a universal gravitational field and stationary atmosphere. The trajectory variables are altitude h; velocity V, flight path angle γ, and the angular range, θ. The equations of motion are

$$\frac{dh}{dt} = V \sin\gamma \tag{6}$$

$$\frac{dV}{dt} = -\frac{\rho V^2}{2\beta} - g\sin\gamma \tag{7}$$

$$\frac{d\gamma}{dt} = -\frac{V\cos\gamma}{R_m + h} - \frac{g\cos\gamma}{V} \tag{8}$$

$$\frac{d\theta}{dt} = \frac{V\cos\gamma}{R_m + h} \tag{9}$$

The ballistic coefficient β in the equations of motion is given by

$$\beta = \frac{m}{C_D A} \tag{10}$$

where, C_D is drag coefficient of the spacecraft and A is the reference surface area of the spacecraft. Since the entry speed is constrained to less than 6.5 km/s while designing the Earth to Mars trajectories, only convective heating is considered [15]. Sutton-Graves relation is used to estimate the convective stagnation-point heating rates [16].

The vehicle in the concept is Phoenix capsule (four of them in total) and is modeled as a point mass. It is a 70-degree half-angle sphere-cone with a base diameter of 2.65 m, and a nose radius of 0.6625 m to compute convective heat rates [17]. The properties for EDL simulation at Mars are summarized in Table 4.

Table 4: EDL simulation properties for Mars.

Properties [Unit]	Value
Mars radius [km]	3376.2 km
Gravitational Parameter [km^3/s^2]	4.2828×10^{13}
Mars-GRAM Year	2005
Ratio of specific heats	1.2941
Sutton-Graves Coefficient [$kg^{0.5}/m$]	1.8980×10^{-4}

A panel method [18] is used to generate the aerodynamic coefficients as a function of the drag skirt length. Since, only ballistic entry is considered aerodynamic coefficients are constant for a particular drag area configuration. The parachute for the secondary spacecraft is a Viking-type disk-gap-band parachute with a diameter of 11.73 m [19]. The Mach number-dependent drag coefficient of parachute used in the Phoenix mission is also used for this concept [19]. Terminal descent systems—retro-rockets or airbag landers are not modeled in this concept. The goal was to bring the two spacecraft in each flight system to terminal speeds such that terminal descent systems could be used for soft landing.

5.1 Extended Heat Shield Sizing

Although three options of drag skirt are considered, in the succeeding analysis, the heat shield extension option is explored. This option represents what is achievable via current technologies. The same methodology can be used to easily explore the other

options—rigid deployable decelerator, and HIAD. The base diameter of the phoenix spacecraft is 2.65 m [17]. Therefore, the maximum allowable length of the drag skirt possible which will fit in to a 5-m payload fairing is found to be around 1.25 m. Using Fig. 14, the value of κ corresponding to this length is around 3 (the drag area of Phoenix spacecraft is around 8.14 m^2 [17]). As the secondary spacecraft is a Phoenix-class vehicle, the corresponding properties of all the vehicle configurations during EDL are summarized in Table 2.

Table 5: Properties of different vehicle configurations.

Properties [Unit]	Value	Comment
η	0.2	
κ	3	
β_s [kg/m^2]	70	Phoenix Spacecraft [19]
β_{fs} [kg/m^2]	38.5	55% of β_s
β_p [kg/m^2]	21	30% of β_s

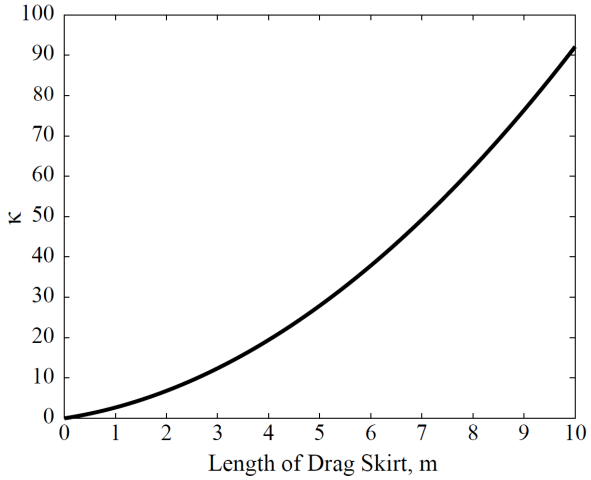

Fig. 5: Variation of drag area vs length of drag skirt. Panel method is used to compute the drag area and therefore κ.

5.2 Corridor Width and Range Capability

The range separation between the two spacecraft—primary and secondary—is influenced by the entry flight path angle, time of secondary spacecraft release, and the ratios of the ballistic coefficients of main and the primary spacecraft to the secondary spacecraft. For a given minimum range separation requirement on surface, the entry corridor in terms of flight path angle is bounded by the cases: steep flight path angle which fulfill the minimum range separation requirement, and the shallow flight path angle resulting in to grazing trajectory which does not escape the Martian atmosphere.

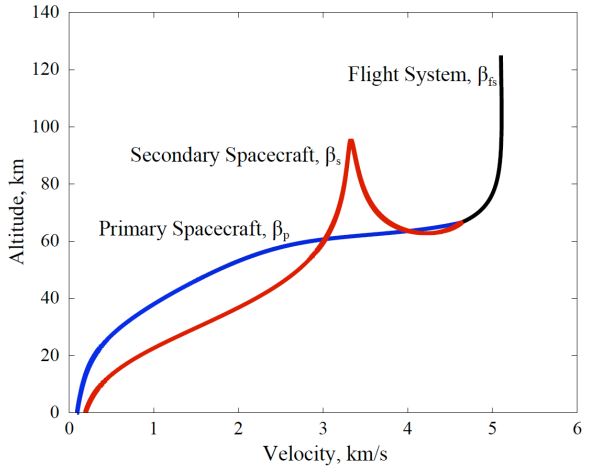

Fig. 6: Altitude versus velocity. Secondary space with a larger ballistic coefficient follows a skip trajectory to attain the desired range separation.

For a particular entry interface (EI) state, secondary spacecraft with maximum β_s characterizes the longest range trajectory, and the primary spacecraft with minimum β_p characterizes the shortest range trajectory. The difference between the two gives the range separation between the two spacecraft. In addition, for a given EI state, the entry flight system (with medium β_{fs}) until the release of the secondary spacecraft also affects the overall range capability. Figs. (14) and (15) shows the bounding trajectories for a given EI state and a minimum range separation requirement of 3000 km.

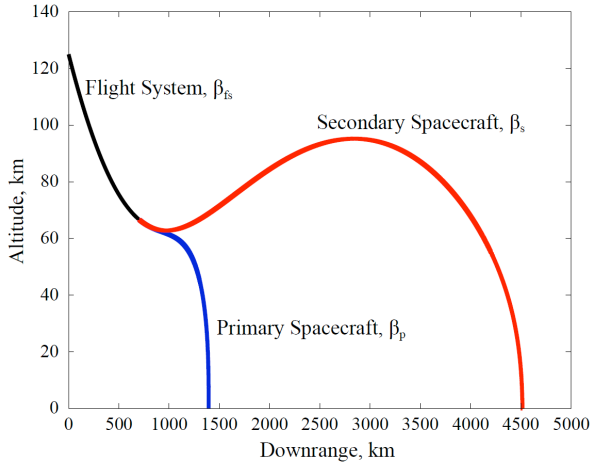

Fig. 7: Altitude versus downrange. Primary spacecraft with low ballistic coefficient lands with a shorter range compared to the secondary spacecraft.

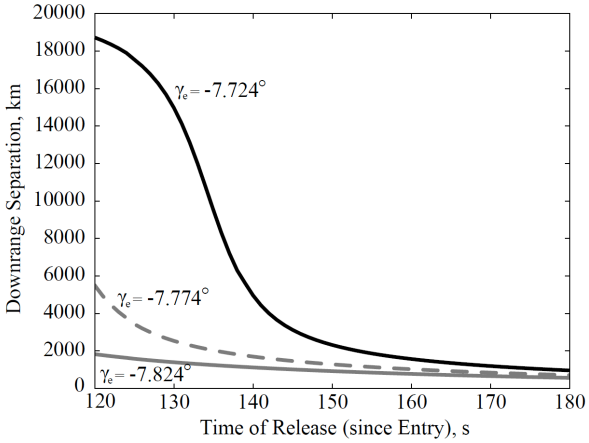

Fig. 8: Spacecraft downrange separation versus release time.

For a given EI state, the range separation can be controlled by regulating the release time (drag modulation event) of the secondary spacecraft. Fig. 16 shows the range separation capability for vehicle configuration given in Table 3 for three different EI flight path angle. It can be seen that for longer range separation requirements, separation is very sensitive to release time. Fig. 16 also shows the sensitivity of range separation capability for entry corridor of 0.05°. Shallow EI flight path angle exhibits extensive range separation capabilities but at the expense of high total heat load for the primary spacecraft. Shorter range separation can be attained by a range of flight path angle and release time. The width of the corridor reduces as the range separation requirement is increased. The range separation goals and release time in turn affects the total heat load and thus the Thermal Protection System (TPS) mass of the primary and secondary spacecraft.

A particular range separation can be attained via steep flight path angle and early release (of secondary spacecraft) or a shallow flight path angle and late release.

5.3 Landing Accuracy

It has been shown that MSL-class landing accuracies (downrange error of ~10 km) are achievable by a guidance algorithm which determines the drag skirt jettison time [20]. A similar guidance strategy can be implemented for this concept to determine the range separation. This will further improve the landing accuracy of both the primary and the secondary spacecraft. However, only ballistic entry is considered in this paper. The concept presents a distinctive capability of drag modulation via reduction in mass (release of a secondary spacecraft) from the main entry flight system. From Table 4, it can be seen that the ballistic coefficient modulation capability is bounded by -45% to +82% compared to β_{fs}. It is worth to mention that even without guidance, only by carefully selecting the EI flight path angle and jettison time, improved landing accuracy (in contrast to Phoenix's case of ~100 km of downrange error) can be obtained. However, with the increase of range separation requirements, the landing error of the secondary spacecraft degrades because of need of a skip trajectory.

6. EDL ASSESSMENT

6.1 Nominal Trajectory

Of the several possible trajectories, the one in year 2033 is used for the assessment of the concept. The EI state of altitude, velocity, and range (longitude for equatorial entry trajectory) corresponds to the Phoenix mission. EI Flight path angle is selected to fulfil the range separation requirements of the two spacecraft.

The range separation between the two spacecraft for the nominal case was found to be 3410 km. The maximum heating rates of the primary and secondary spacecraft are found to be 26.6 W/cm^2 and 28.2 W/cm^2 respectively. The maximum deceleration at secondary release is around 2.6g.

6.2 Monte Carlo Simulations

Monte Carlo approach was used to perform statistical analysis on the entry, descent, and landing concept in the presence of uncertainties. Using the dispersions outlined in Table 6, sets of 1000 trajectories were propagated to determine the feasibility and robustness of this concept and its sensitivities to the dispersions. Performance indicators of the Monte Carlo results show the feasibility of this alternative EDL concept.

Fig. 9 shows the dispersed landing points of the primary and the secondary spacecraft. For this Monte Carlo run, the release of secondary spacecraft is biased to occur at or after peak heating of the flight system. Release of secondary spacecraft after peak heating reduces the heating rate and total heat load on the secondary spacecraft. To achieve that, a shallow EI flight path angle is selected and secondary is released late. Fig. 10 shows the corresponding landing separation and error of both the primary and secondary spacecraft of flight system 1 and 2 projected on Mars

surface as seen from the North Pole. To land four landers, retrograde and posigrade entries for flight system 1 or 2 can be selected as shown in Fig. 18 to have downrange separation of at least 3000 km between each lander.

Table 6: Parameters and inputs for Monte Carlo simulations.

Parameter	Units	3-σ dispersion	Reference
Atmosphere		Model	
Velocity	m/s	0.439	[21]
Flight path angle	deg	0.0003	
Altitude	m	0	
Range angle	deg	0.002	
Mass	kg	0.5	
Drag area	m^2	3%	
Release time (since EI)	s	2	

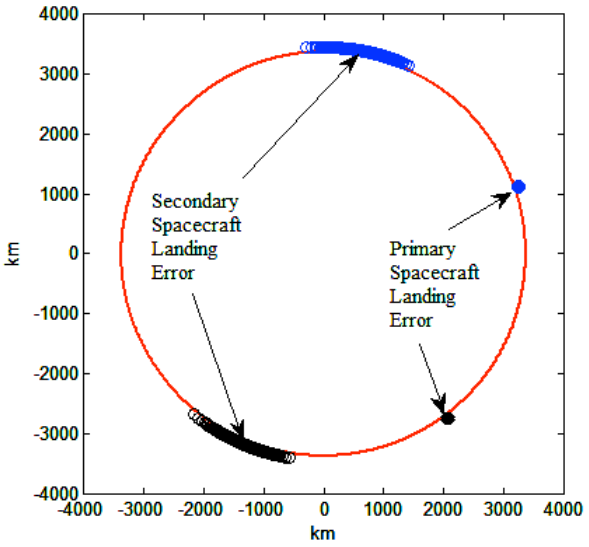

Fig. 11: Landing error of primary and secondary spacecraft projected on Mars's surface.

The maximum convective heating for the flight system (or the primary spacecraft) during the hypersonic phase is 27.4 ± 0.4 W/cm^2 (all number after ± are 3-σ values) occurs at approximately 5.1 km/s (Fig. 22). This is a 55% reduction in heating rate as compared to Phoenix mission limit (<64 W/cm^2) [19]. Thus, heritage SLA561V heat shield material can be used as TPS with significant reserve margin.

The maximum deceleration at secondary release is around 2.6g. Post-release the low β_p primary spacecraft's deceleration increased to a maximum of 5.8g ± 0.4g but the high β_s secondary spacecraft reduces to a maximum of 2.2g ± 0.3g prior to parachute deployment (Fig. 15). The shallow EI flight path angle reduces the overall peak deceleration of the three entry

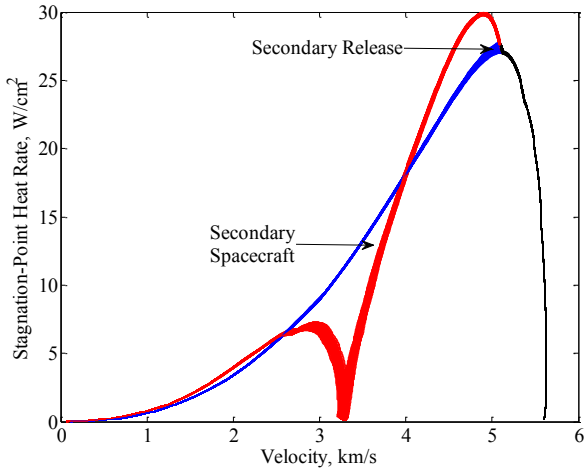

Fig. 12: Stagnation heat rate versus velocity.

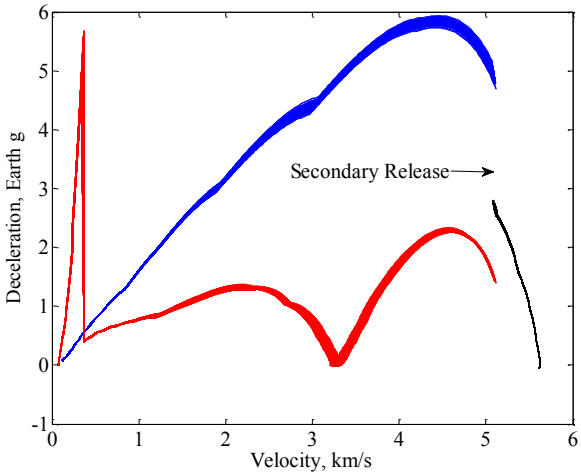

Fig. 13: Deceleration versus velocity.

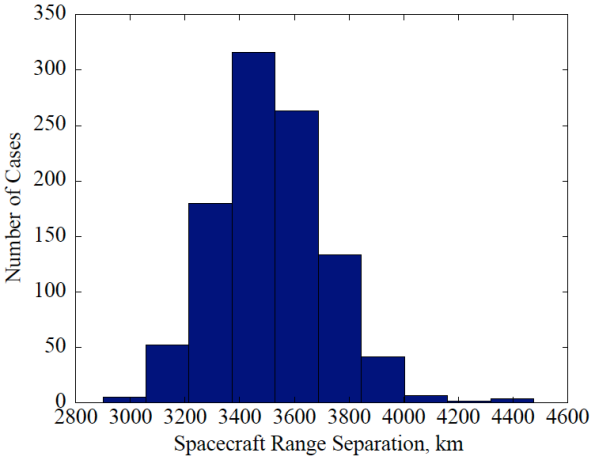

Fig. 14: Spacecraft downrange separation distribution.

configurations and also at secondary release. Due to relatively low deceleration at secondary release it is assumed that a lateral maneuver using thruster or other means can release the secondary from the flight system. However, this maneuver is not modelled in this paper.

For this Monte Carlo run, out of 1000 cases, 5 cases violated the range separation requirements of at least 3000 km between the primary and secondary spacecraft (Fig. 16). Another Monte Carlo run with a proper combination of shallow flight path angle and early secondary release will satisfy the range separation requirements. The sensitivity of this EDL concept to EI flight path angle and release time for longer range separation requirements (>3000 km) is high. The range separation is found to be 3513 ± 595 km downrange.

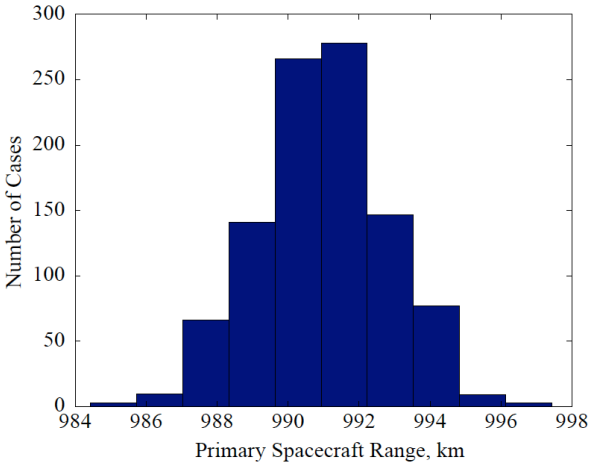

Fig. 17: Primary spacecraft range distribution.

For the dispersions outlined in Table 5, the terminal landing accuracy of the primary spacecraft is very high—16 km in 3-σ downrange error, as shown in Fig. 25. However, this landing accuracy of the primary spacecraft comes at the expense of the low landing accuracy of secondary spacecraft—4504 ± 600 km downrange (all number after ± are 3-σ values), as shown in Fig. 26. This large error is due to skip trajectory required to attain the long range separation requirements of 3000 km. While this error is large, the requirement of landing four landers with a separation of at least 3000 km is fulfilled.

The large downrange error of the secondary spacecraft is small for low range separation requirements. If the secondary can be released late (low range separation requirement) then its landing accuracy is improved. However, releasing the secondary late i.e. flying with medium β_{fs} for longer duration increases the landing error of the primary. Hence, the right selection of release time is important based on the mission requirements. Early release ensures the primary descends with the lowest β_p, and higher is its landing accuracy.

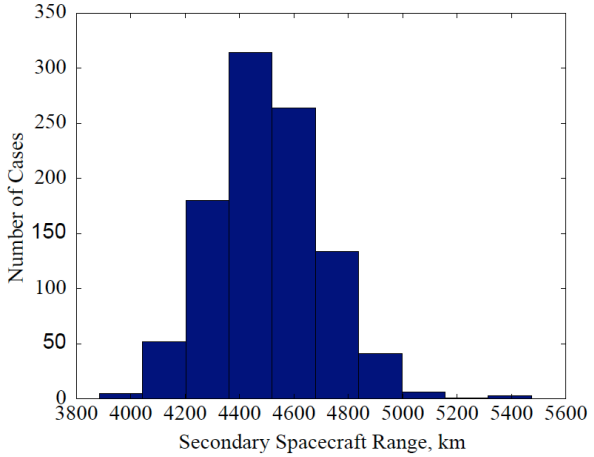

Fig.26: Secondary spacecraft range distribution.

For the vehicle properties defined in Table 6, in the case of very low ballistic coefficient of the primary spacecraft ($\beta_p = 21\ kg/m^2$) no supersonic parachute is required. In the Monte Carlo simulation, the terminal speed of the primary spacecraft without parachute is 112 m/s. The terminal speed of the secondary spacecraft with Viking-type disk-gap-band parachute is 62 m/s (and around 190 m/s without parachute). Retrorockets and airbag systems for terminal descent and landing can counter these terminal speeds.

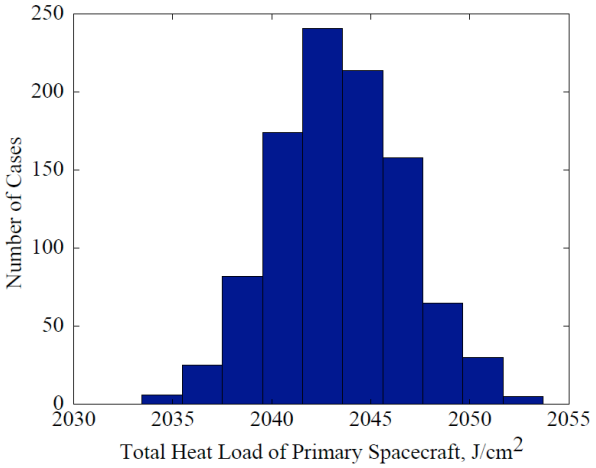

Fig.27: Primary spacecraft integrated (total) heatload distribution.

The integrated heatload of the primary spacecraft is 2042 ± 48 J/cm^2 and that of the secondary spacecraft is 3985 ± 48 J/cm^2. The heat load of the primary includes the heat load of the portion of the entry trajectory prior to the secondary spacecraft release. Therefore, even

though a shallow EI flight path angle is required to achieve the landing separation requirement, the integrated heat load of each of the spacecraft is similar to or almost half of that of the Phoenix spacecraft.

The Thermal Protection System Mass Fraction (μ_{tps}) strongly depends on integrated heat load is computed using the empirical relation given by

$$\mu_{tps} = 0.091 \times (q_{load})^{0.51575} \quad (11)$$

where, q_{load} is the integrated heat load. The empirical relation is computed by fitting the TPS mass fraction of the previous Mars' mission with the respective integrated heat load. The % TPS for the primary spacecraft is found to be around 4.63% with around 0.05% of 3σ dispersions as seen in Fig. 18. Out of this, 50% is contributed by the portion of the trajectory prior to the secondary release. The TPS mass fraction for the secondary spacecraft is 6.84%). The TPS of the primary can be reduced by selecting a steep EI flight path angle and releasing the secondary spacecraft early.

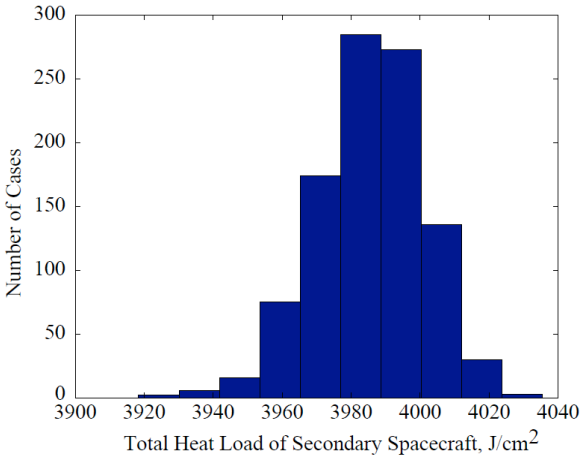

Fig.28: Secondary spacecraft integrated (total) heatload distribution.

7. DISCUSSION

Both of the methods—using Centaur or Solar Electric Propulsion—to get a separation of 7 days between the two Flight Systems have their advantages. Using the Centaur upper stage to perform the separation uses less propellant and is less complicated (i.e. no extra propulsion system is required). However, the low thrust method has significantly lower arrival V_∞ at Mars, thereby enabling the delivery of increased payload mass to altitude that may not be possible otherwise. The low-thrust method represents an attractive option for any future mission to Mars to reduce the entry velocity and to enable the delivery of larger payloads. Low-thrust propulsion also enables landing at higher elevations.

Low velocities of the spacecraft also present benign aerothermal environments compared to past Mars missions. A supersonic decelerator (parachute) is not required due to the low ballistic coefficient of the primary spacecraft.

The proposed architecture presents increased risks associated with (a) the separation of the two flight systems, and (b) the separation of the two spacecraft from a flight system inside the atmosphere. The risks associated with this concept are expected to be less than if four landers were launched and placed individually.

Although the total system mass increases—due to the need of an extra spacecraft adapter and release mechanism—the reduction in the number of cruise stages and parachutes offsets a significant fraction of that increase in mass.

This architecture requires only a single Atlas V 541 launch, as opposed to other concepts which require two Atlas V 401 launches or four Delta II 7925 launches, to deliver four Phoenix-class landers to Mars. Therefore, this concept can result in the significant reduction of total launch cost.

8. OTHER POTENTIAL APPLICATIONS

There are several other potential applications of this concept. This architecture can be used to deliver multiple payloads for Mars network science missions where the lander range separation requirement is shorter. For range separation of 200 km or less, the secondary spacecraft need not have any kind of thermal protection, thereby resulting in significant savings in TPS mass. For range separation up to 700 km less than 5.0% of TPS is required for the secondary spacecraft.

Table 7: Other potential applications of the concept. Primary landing error is less than 10 km. Footnote a Primary % TPS is ranges from 11 to 13%. Footnote b

Range Sep., km	FPA	Release Time	2nd Landing Error, km	Total Heat Load	Maximum Stagnation Point Heating, W/cm^2
1054	-10.2°	122	60	2900	28
346	-10.8°	122	15	1310	28
140	-10.8°	144	12	425	11

705	-10.0°	144	45	2004	28
270	-10.0°	164	13	806	13

Instead of two landers, the concept may be used to deliver a pair of orbiter-lander to Mars orbit and surface respectively.

This architecture also provides an alternative approach in which c.g. offset for lift control through bank-to-steer approach may be created by the release of a secondary spacecraft instead of releasing dead masses which was done for the Mars Science Laboratory mission. This will result in increased science payload for a given spacecraft entry mass and open up possibilities of delivering multiple spacecraft on to Mars surface.

9. REFERENCES

1. Vision and Voyages for Planetary Science in the Decade 2013-2022, Committee on the Planetary Science Decadal Survey; National Research Council, National Research Council, Washington D.C., 2011.
2. Jeffrey R. Johnson, et al. Mars Science Goals, Objectives, Investigations, and Priorities, Mars Exploration Program Analysis Group (MEPAG), September 24, 2010.
3. J. L. Counil, F. Ferri, Ph. Lognonne, O. Marsal, F. Rocard, and R.Bonneville., The NetLander Mission: A Geophysical Network Aimed at Investigating Mars Atmosphere, Sub-surface and Deep Interior, Conference on the Geophysical Detection of Subsurface Water on Mars, Lunar and Planetary Institute, Houston, Texas August6-10, 2001.
4. Agustin F. Chicarro, et al., MNSM – A Future Mars Network Science Mission, 43rd Lunar and Planetary Science Conference, The Woodlands, Texas, March 19-23, 2012.
5. A.-M. Harri, et al. MetNet—In Situ Observational Network and Orbital Platform to Investigate the Martian Environment, Finnish Meteorological Institute Space Research, Helsinki 2007.
6. Lindy Elkins-Tanton, et al., Mission Concept Study, Planetary Science Decadel Survey Mars Geophysical Network, NASA HQ, June 2010.
7. W. Bruce Banerdt, et al., InSight—Geophysical Mission to Mars, Mars Exploration Program Analysis Group (MEPAG), 4 October, 2012.
8. Mark Wilkins and George Powers, Atlas V Launch Services User's Guide, United Launch Alliance, Centennial, CO, March 2010.
9. J. L. Prince, P. N. Desai, E. M. Queen, and M . R. Grover., Mars Phoenix Entry, Descent, and Landing Simulation Design and Modeling Analysis, *Journal of Spacecraft and Rockets*, Vol. 48, No. 5, September-October 2011.
10. M. E. Tauber and K. Sutton, Stagnation-Point Radiative Heating Relations for Earth and Mars Entries, *Journal of Spacecraft and Rockets*, Vol. 28, June 2003, pp. 40-42.
11. Rinderle, E., Galileo User's Guide, MIssion Design System, Satellite Tour Analysis and Design Subsystem," Jet Propulsion Laboratory, California Institute of Technology, Pasadena, CA, JPL Internal Document D-263.
12. Sims, J. A., Finlayson, P. A., Rinderle, E. A., Vavrina, M. A., and Kowalkowski, T. D., "Implementation of a Low-Thrust Trajectory Optimization Algorithm for Preliminary Design," AIAA Paper 2006-6746, Aug. 2006.
13. Gill, P. E., Murray, W., and Saunders, M. A., "SNOPT: An SQP Algorithm for Large-Scale Constrained Optimization," *SIAM Journal on Optimization*, Vol. 12, 2002, pp. 979–1006.
14. Marc D. Rayman, et al., Dawn:Amission in development for exploration of main belt Asteroids Vesta and Ceres, *Acta Astronautica* 58 (2006) 605 – 616.
15. Robert D. Braun and Robert M. Manning, Mars Exploration Entry, Descent, and Landing Challenges, *Journal of Spacecraft and Rockets,* Vol. 44, No. 2, March-April 2007.
16. K. Sutton and R. A. Graves, A General Stagnation-Point Convective-Heating Equation for Arbitrary Gas Mixtures, Technical Report, NASA TR R-376, NASA, Washington, DC, November 1971.
17. Karl T. Edquist, et al., Aerodynamics for the Mars Phoenix Entry Capsule, *Journal of Spacecraft and Rockets*, Vol. 48, No. 5, September–October 2011.
18. J. D. Anderson Jr., *Fundamentals of Aerodynamics*, McGraw Hill, ISBN-13**:** 978-0073398105, February 12, 2010.
19. J. L. Prince, et al., Mars Phoenix Entry, Descent, and Landing Simulation Design and Modeling Analysis, *Journal of Spacecraft and Rockets*, Vol. 48, No. 5, September-October 2011.
20. Z. R. Putnam and R. D. Braun, Precision Landing at Mars Using Discrete-Event Drag Modulation, 23rd AAS/AIAA Space Flight Mechanics Meeting, Kauai, Hawaii, February 10-14, 2013.
21. R. C. Blanchard and P. N. Desai, Mars Phoenix, Entry, Descent, and Landing Trajectory and Atmosphere Reconstruction, *Journal of Spacecraft and Rockets,* Vol. 48, No. 5, September-October 2011.